CARBON letters

Original Articles
Carbon Letters Vol. 24, 82-89 (2017)

Physicochemical properties and methane adsorption performance of activated carbon nanofibers with different types of metal oxides

Faten Ermala Che Othman[1], Norhaniza Yusof[1,*], Hasrinah Hasbullah[1], Juhana Jaafar[1], Ahmad Fauzi Ismail[1] and Noor Shawal Nasri[2]

[1]Advanced Membrane Technology Research Center (AMTEC), Faculty of Chemical & Energy Engineering, Universiti Teknologi Malaysia, Johor Bahru 81310, Malaysia
[2]UTM-MPRC of Oil and Gas Institute, Faculty of Chemical & Energy Engineering, Universiti Teknologi Malaysia, Johor Bahru 81310, Malaysia

Article Info

Received 8 May 2017
Accepted 24 August 2017

***Corresponding Author**
E-mail: norhaniza@petroleum.utm.my
Tel: +6075535388

Open Access

DOI: http://dx.doi.org/10.5714/CL.2017.24.082

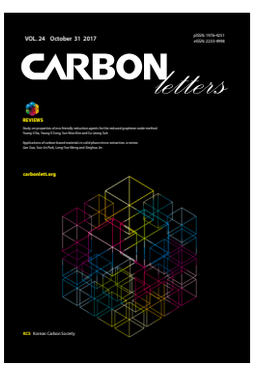

http://carbonlett.org

pISSN: 1976-4251
eISSN: 2233-4998

Abstract

In this study, composite PAN-based ACNFs embedded with MgO and MnO_2 were prepared by the electrospinning method. The resultant pristine ACNFs, ACNF/MgO and ACNF/MnO_2 were characterized in terms of their morphological changes, SSA, crystallinity and functional group with FESEM-EDX, the BET method, XRD and FTIR analysis, respectively. Results from this study showed that the SSA of the ACNF/MgO composite (1893 $m^2 g^{-1}$) is significantly higher than that of the pristine ACNFs and ACNF/MnO_2 which is 478 and 430 $m^2 g^{-1}$, respectively. FTIR analysis showed peaks of 476 and 547 cm^{-1}, indicating the presence of MgO and MnO_2, respectively. The FESEM micrographs analysis showed a smooth but coarser structure in all the ACNFs. Meanwhile, the ACNF/MgO has the smallest fiber diameter (314.38±62.42 nm) compared to other ACNFs. The presence of MgO and MnO_2 inside the ACNFs was also confirmed with EDX analysis as well as XRD. The adsorption capacities of each ACNF toward CH_4 were tested with the volumetric adsorption method in which the ACNF/MgO exhibited the highest CH_4 adsorption up to 2.39 mmol g^{-1}. Meanwhile, all the ACNF samples followed the pseudo-second order kinetic model with a R^2 up to 0.9996.

Key words: activated carbon nanofibers, magnesium oxide, manganese dioxide, methane adsorption

1. Introduction

Recently, most of our vehicles run on either gasoline or diesel fuel, which is unsafe and an environmental hazard [1]. To protect the earth from these dangerous pollutants, a clean and efficient energy such as natural gas (NG) has attracted much attention because it produces less pollution compared to fossil fuels. Unlike fossil fuels, NG burns cleanly and releases less carbon dioxide. However, NG has a low volumetric energy density which limits the transportation process and its gas storage capacities [2].

Previously, researchers have done many studies on using the compressed natural gas (CNG) method for gas storage. Nevertheless, this method has some disadvantages because NG is required to be stored under a maximum pressure of about 20–25 MPa as a compressed supercritical fluid at room temperature [3], which is risky and costly. To overcome these problems, many recent studies have focused on absorbed natural gas (ANG) as an alternative way of gas storage because porous adsorbent materials are able to store NG at a relatively low pressure, approximately about 3.5–4 MPa at room temperature [4]. Due to their high energy density capability, the flexibility of the fuel tank, lighter weight of the pressure vessels

and their cost-effectiveness, ANG technologies have become a great competitor to CNG and liquefied natural gas (LNG) technologies [5].

One excellent example of adsorbent implied for ANG technologies is activated carbon nanofibers (ACNFs) due to their porous carbonaceous structures, non-hazardous properties and readily-processability [6]. With their diameters in the nanometer range (10–1000 nm) together with a large surface area and concomitant high adsorption capacity [7], ACNFs have become optimal candidates for various major applications like environmental engineering, energy storage and biotechnology. Due to its uniqueness and versatility, ACNFs have manifested more interests and attention in diverse research fields either in ongoing or future studies.

Therefore, electrospinning is a simple and interesting method that can be used to produce a fine ACNF with a smaller diameter and more developed micropores. ACNFs are commonly prepared by electrospinning followed by a suitable pyrolysis process. During the electrospinning process, NFs with diameters ranging from several micrometers to nanometers are produced by the electrostatic forces. Electrospinning has become one of the most preferred techniques in fabricating NFs either on an industrial or laboratory scale because the system is simple and economical as well as has a comparatively high rate of production. The NFs then undergo the three steps of the pyrolysis process, which are stabilization in an oxidizing condition, carbonization in an inert condition and activation, either physically or chemically. The optimum conditions for the pyrolysis of nanofibers have been reported in earlier studies [8,9].

Although polyacrylonitrile (PAN)-based ACNFs have shown good properties, it is believed that the impregnation of metal oxides as additives could increase the specific surface area (SSA) of ACNFs as well as the pore volume. These characteristics are very important for ACNFs to become good adsorbent materials especially in ANG technology because this type of adsorbent can store NG at a higher amount at a relatively low pressure and is also safer compared with the CNG and LNG storage methods. Thus, the aim of this study was to prepare PAN-based ACNFs with different types of metal oxides by electrospinning and further activation processes. The resultant ACNFs were evaluated in terms of their physicochemical changes and adsorption capability. ACNF composites could serve as another potential alternative to CH_4 adsorbents.

2. Experimental

2.1. Fabrication of nanofibers

N,N-dimethylformamide (DMF), PAN, magnesium oxide (MgO) and manganese dioxide (MnO_2) nanoparticles were directly purchased from Sigma-Aldrich (USA). The predetermined amount of metal oxide nanoparticles (1% relative to the total weight) were introduced into DMF for at least 5 h followed by the addition 10% PAN (total weight) into the solution. The mixture was mechanically stirred for 24 h to obtain homogeneous solutions [10]. All the PAN-based NFs were fabricated by the electrospinning method. The electrospinning process was done by optimizing the parameters [11,12]: an infusion rate of 1 mL h^{-1}; a needle to collector distance of 20 cm, and a voltage of 15 kV.

2.2. Activation of the nanofibers

All the resultant NFs were subjected to the pyrolysis process with a tube furnace (Carbolite model CTF 12/65/550). The NFs were first stabilized by treating the samples in an oxygen- rich environment at a temperature of 275°C with a ramping rate of 2°C/min for a 30 min residence time. The precursor NFs were then carbonized up to 600°C for 65 min in a high-purity nitrogen gas with a flow rate of 0.2 L min^{-1} and a ramping rate of 5°C/min. The carbonized NFs (CNFs) then were activated by introducing the CNFs to a carbon dioxide gas with a 0.2 L min^{-1} flow rate until 800°C for 40 min to obtain the ACNFs. The resultants samples were denoted as ACNF, ACNF/MgO and ACNF/MnO_2 which represent the pristine ACNFs and ACNFs filled with MgO and MnO_2, respectively.

2.3. Characterization

The morphology, diameter and elemental compositions of the resultant ACNFs were analyzed with field-emission scanning electron microscopy (FESEM) coupled with energy dispersive X-ray (EDX) spectroscopy (JEOL JSM-5610LV, Japan). Fourier transform infrared spectroscopy (FTIR) spectra of the KBr powder-pressed pellets were recorded on a FTIR-2000, PerkinElmer spectrometer from 400 to 4000 cm^{-1} to determine the chemical bonds and surface functional groups (USA). X-ray diffraction (XRD) patterns were detailed at $2\theta=2–90^{o}$ obtained with an XRD (D8 Advance diffractometer; Bruker, USA) using Cu Kα radiation to investigate the elemental analysis of the samples because it provides information about the crystalline structure of the ACNFs [13]. The pore structures and the adsorption isotherms of the porous ACNFs were identified with Micromeritics ASAP 2000 at –196°C by adsorption of liquid nitrogen. The SSA was calculated according to the Brunauer-Emmett-Teller (BET) method at the relative pressure (P/P_o) range of 0.04–0.2, and the pore volume was determined from the amount of nitrogen adsorbed at $P/P_o=0.99$ [14].

2.4. CH_4 volumetric adsorption test

In this study, the CH_4 uptake for each sample was tested with a custom-made adsorption rig with a simple static volumetric measurement method. This unit is basically equipped with an adsorption cell (AC) and loading cell (LC), a vacuum pump, a K-type thermocouple (to monitor the temperature changes inside the cells) and a digital pressure transducer (to monitor the pressure changes in both the AC and LC). Each particular ACNF was loaded into the AC while CH_4 was loaded into the LC until the pressure reached the required levels which are 3.5 bar. Because the pressure was set to the desired levels, the experiment was initiated by opening the valve between the LC and AC to introduce CH_4 with the ACNFs (adsorbent) in the AC. The pressure changes in both cells were recorded continuously at 5 min intervals until the equilibrium pressure was achieved. The equilibrium state was determined when both the temperature and pressure were constant for approximately 10 min. The amount

of CH_4 adsorbed was calculated with the following equation:

$$q = \frac{1}{m}\left[\frac{Vv}{R}\left(\left|\frac{P}{ZT}\right| i - \left|\frac{P}{ZT}\right| eq\right) a + \left(\left|\frac{P}{ZT}\right| i - \left|\frac{P}{ZT}\right| eq\right) l\right]$$

, where P is the pressure (bar), T is the temperature (K); V is the volume (cm^3); R is a gas constant; a is the adsorption cell (g); l is the loading cell (g); i and eq represent the initial state and the adsorption final equilibrium state, respectively; m is the adsorbent mass (g), and q is the amount of gas adsorbed (mol g^{-1}). Z is the compressibility factor [15].

Moreover, the CH_4 uptake versus time was simulated by the pseudo-first and pseudo-second order kinetic models.

3. Results and Discussion

3.1. Morphology and diameter of the ACNFs

The FESEM images of the ACNFs with the different types of metal oxides are shown in Fig. 1. The surfaces of all ACNFs were typically smooth but with some irregular and flexuous fibrous morphology, for which the diameter of the ACNFs incorporated with metal oxides had a smaller diameter ranging between 314.38±62.42 and 327.86±35.08 nm compared to the pristine ACNFs (356.67±92.19 nm). After activation, the diameter of the ACNFs seems to decrease from their original shape due to material shrinkage. This shrinkage is related to the breakage of the hydrogen bond and also to the surface vulnerability to heat treatment during stabilization resulting in more weight loss [16]. Consequently, a significant smaller fiber diameter and porous structure were obtained.

The decrease in diameter of the ACNFs after activation is due to the reactions during the thermal stabilization and activation steps. Both modified ACNFs show a uniform distribution of metal oxides (beads-free structures) and possess a smaller diameter compared to the pristine ACNFs. This might be due to the catalytic effect of the metal oxides themselves which can dissociate during the heat treatment.

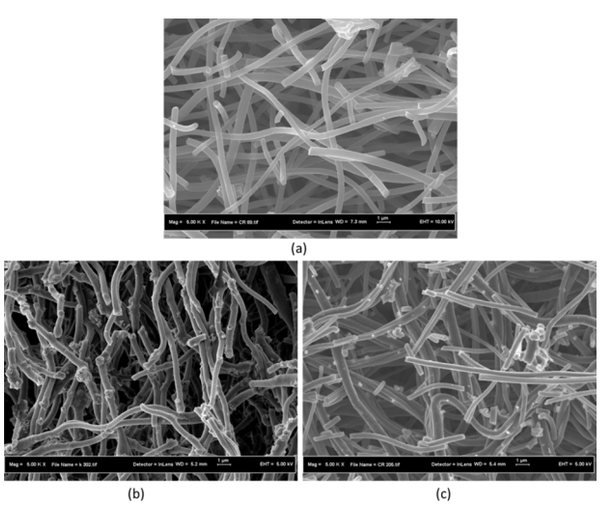

Fig. 1. Field-emission scanning electron microscopy images of pristine ACNFs (a), ACNF/MgO (b), and ACNF/MnO_2 (c) at ×5000 magnification. ACNFs, activated carbon nanofibers.

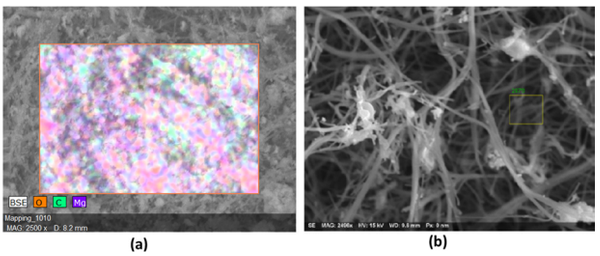

Fig. 2. Energy dispersive X-ray images of the modified activated carbon nanofibers with MgO (a) and MnO_2 (b).

Table 1. Atomic percentages of the elements in ACNF/MgO and ACNF/MnO_2

Sample	ACNF/MgO (at%)	ACNF/MnO_2 (at%)
C	47.18	69.24
O	36.20	30.22
Mg/Mn	16.62	0.54

ACNF, activated carbon nanofiber.

The EDX imaging analysis revealed the surface structure of the materials and the distribution of the local elements for the modified ACNFs shown in Fig. 2. This EDX analysis confirmed that the white and spongy appearance in Fig. 2a and b indicates the presence of Mg and Mn on the ACNFs. It was observed in Fig. 2 that the carbon element was present at a high percentage in both samples followed by oxygen and magnesium (Mg) and manganese (Mn). A very high amount of carbon content was obtained, and this typically is due to the carbonization of the polymer PAN. On the other hand, the high oxygen content is due to the oxidation of the polymer with air and the formation of carbonyl and hydroxyl groups. The existence of Mg and Mn at low percentages on the surface of the ACNFs (especially for Mn) after impregnation of the element was also established; however, this proved the success of the impregnation process. This could possibly be due to the oxidation or degradation of the MnO_2 during the high temperature treatment because MnO_2 itself has a low melting point (535°C). The elements detected by the EDX analyzer with their respective atomic percentages are presented in Table 1. The table shows that the presence of Mg and Mn on the surface of the ACNFs was about 16.62% and 0.54%, respectively.

3.2. Textural properties of ACNFs

The SSA of the ACNFs is remarkably increased after undergoing activation at a high temperature. As can be seen in Fig. 3 and Table 2, the range of the SSA of all the ACNFs samples ranged between 430.87 to 1893.09 $m^2 g^{-1}$, for which ACNF/MgO has the largest SSA compared to the other ACNFs. However, the SSA of the pristine ACNFs is much higher compared with ACNF/MnO_2 which is opposite to the theoretical statement. The SSA of ACNFs incorporated with

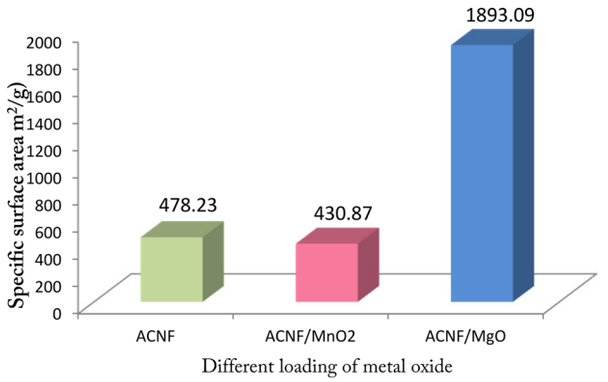

Fig. 3. Comparison of the specific surface area of the activated carbon nanofibers (ACNFs) with different types of metal oxides.

a metal oxide should be higher; however, the SSA of ACNF/MnO_2 is lower compared to the pristine ACNFs, and this was assumed to originate from too much MnO_2 loaded into the ACNFs which could lead to an uneven contribution of the MnO_2 consequently blocking the pores. For that reason, the presence of beads blocked the porous structure of the NFs leading to a smaller SSA. In this study, both MnO_2 and MgO were directly purchased from a supplier with a particle size of <10 μm and <50 nm, respectively. As can be seen, the particle size of MnO_2 is much bigger than the pore size of the ACNFs, and due to this, the MnO_2 cannot disperse well inside the pores of the ACNFs. Even worse is that it blocked the existing pores that were created during the activation of the carbon making the surface area of the modified-ACNFs with MnO_2 smaller compared to the pristine ACNFs.

In addition, the viscosity, concentration, surface tension, etc. [17] are also believed to be responsible for the existence of the droplet and beads due to the agglomeration of MnO_2 outside the NFs (as can be seen in Fig. 1c), for which the MnO_2 nanoparticles hypothetically should be inside the NFs. In comparison, the SSA of the pristine ACNFs is higher because there are no beads that blocked the pores. Thus, for various reasons, the optimum metal oxide loading is worth investigating to obtain ACNFs with a high SSA.

Table 2 shows the variation of the SSA, pore size, total pore volume (TPV) and V_{micro} of the pristine ACNFs, ACNF/MgO and ACNF/MnO_2. Obviously, the ACNF/MgO possesses the highest TPV and V_{micro} compared to the other ACNFs. It is believed the rise in V_{micro} and the widening of micropore sizes have an important role in the creation of new micropores which would increase the surface area. In fact, the ACNFs with a greater V_{micro} possessed the ability to adsorb considerably higher small particles and molecules such as gases, which in return make them a suitable adsorbent for gas storage and separation applications [18]. Based on the results obtained, ACNF/MgO with the greatest V_{micro} among all the ACNFs could be a potential adsorbent with a high gas storage capacity.

Fig. 4 shows the nitrogen adsorption isotherms of the PAN-based ACNFs prepared with different loadings of metal oxides, and according to the International Union of Pure and Applied Chemistry (IUPAC) classification, the isotherms of the ACNFs are typical type II which represent the abundance of micropores and mesopores in the porous structure (indicated by the long plateau). The graph plotted in Fig. 4 shows that the adsorption of nitrogen was complete at a relatively low pressure which was about 0.1 bar. As can be seen with the ACNF/MgO, at low pressures, the steep rise of the initial slope of the adsorption isotherms indicates the domination of the micropore structure [19] but differs with the pristine ACNFs and ACNF/MnO_2 which show only a slow rise in the graph plotted. Due to the different metal oxides used, the specific adsorption quantity of nitrogen differs greatly (especially between the pristine and ACNF/MnO_2 with ACNF/MgO), implying a difference in the pore and texture structure. Furthermore, all of the samples have a dual-mode pore structure which contains both micropores and mesopores in the porous structures.

Fig. 4 also shows the quantity of nitrogen (N_2) adsorbed by the pristine and modified ACNFs which approached a significant quantity of 110 and up to 513 $cm^3\ g^{-1}$, respectively. It is interesting to note that the lowest quantity of adsorbed N_2

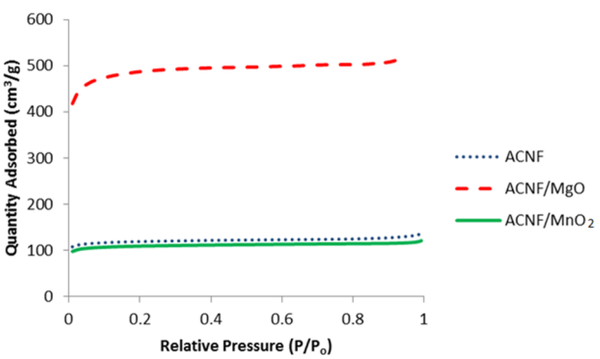

Fig. 4. Nitrogen adsorption isotherms of the PAN-based activated carbon nanofibers (ACNFs) prepared with different loadings of metal oxides. PAN, polyacrylonitrile.

Table 2. Surface area, pore size, TPV and V_{micro} of the pristine ACNFs, ACNF/MgO and ACNF/MnO_2

Sample	BET SSA ($m^2\ g^{-1}$)	Pore size ($cm^3\ g^{-1}$)	TPV ($cm^3\ g^{-1}$)	V_{micro} ($cm^3\ g^{-1}$)
ACNF	478.2298	0.1939	0.2097	0.1593
ACNF/MgO	1893.0871	0.7336	0.62117	0.62117
ACNF/MnO_2	430.2298	0.1723	0.1861	0.1522

TPV, total pore volume; V_{micro}, micropore volume; ACNF, activated carbon nanofiber; BET, Brunauer-Emmett-Teller; SSA, specific surface area.

was achieved by ACNF/MnO_2 followed by the pristine ACNFs. This finding is in agreement with the BET surface area showing the SSA of the ACNF/MnO_2 is the lowest compared to the other ACNF samples. It is believed a low SSA and open pore structure in the ACNFs limit the adsorption capabilities. A significant quantity of N_2 at 512 cm^3 g^{-1} was adsorbed by the ACNF/MgO.

3.3. Chemical bond studies

The spectrum for the pristine ACNFs, ACNF/MgO and ACNF/MnO_2 displayed bands with their respective functional groups shown in Fig. 5. Theoretically, the transition compounds were expected to be removed, and only carbon and hydrogen will remain after activation shown in the figure. There are several peaks located at 2344, 1770, 1554, and 1103 cm^{-1} which represent the different bonds present in the ACNFs. The presence of the alkene groups (C≡C) can be detected at 2344 cm^{-1} while 1770, 1554, and 1103 represent C=O stretching, aromatic C=C bending, and C-H stretching, respectively. The characteristic bands within the range of 550–430 cm^{-1} and 530 cm^{-1} are expected to be the Mg-O and Mn-O bonds, respectively [21,22].

3.4. X-ray diffraction analysis

The XRD patterns of all the ACNF samples showed one strong peak at 13.2° and one broad peak at 26.7° which were attributed to the (002) diffraction of the graphitic crystallites and graphite basal plane, respectively [22,23]. In addition, three strong peaks at 42.9, 62.5, and 78.9° in both modified ACNFs (contained MgO and MnO_2) can be observed [22,24]. These peaks represent the appearance of MgO and MnO_2 inside the ACNFs. These factors jointly result in a change in the morphology, size and texture of the ACNF evident by the FESEM, FTIR and nitrogen adsorption results discussed above (Fig. 6).

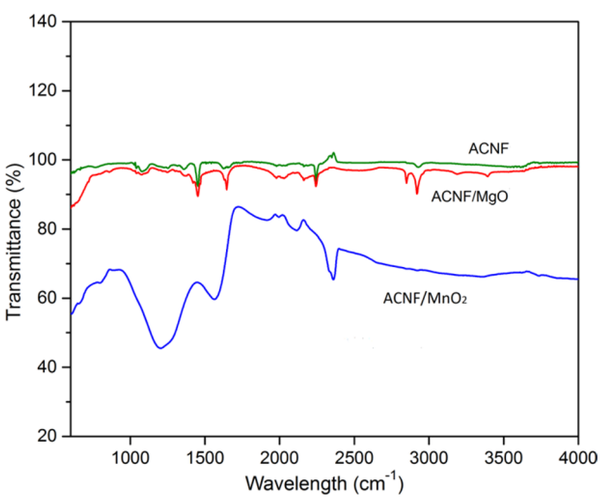

Fig. 5. Fourier transform infrared spectroscopy spectrum of the activated carbon nanofibers (ACNFs) loaded with different types of metal oxides.

3.5. CH_4 volumetric adsorption test

Fig. 7 shows the variation in the amount of CH_4 adsorbed by the different ACNF samples to reach equilibrium versus time at a pressure between 0.5 and 3.5 bar. The adsorption of CH_4 is believed to increase with the contact time. From the graph plotted in Fig. 7, it clearly can be seen that ACNF/MgO has the highest CH_4 uptake of 2.39 mmol g^{-1} followed by ACNF (1.42 mmol g^{-1}) and ACNF/MnO_2 (1.35 mmol g^{-1}). At first, the adsorption of CH_4 increased rapidly and then became slower as the equilibrium was approached, and this slow adsorption is possibly due to the lack of available open sites for CH_4. It can be seen that the ACNFs modified with MgO have a great impact on the CH_4 storage capacity due to the differences in the SSA and pore volumes.

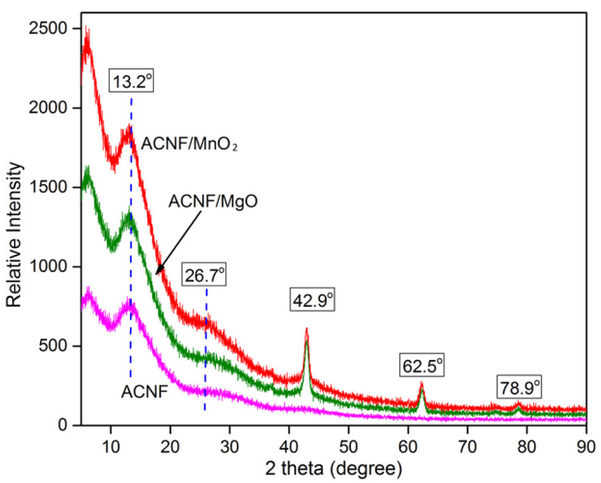

Fig. 6. The X-ray diffraction patterns of the pristine and modified activated carbon nanofibers (ACNFs).

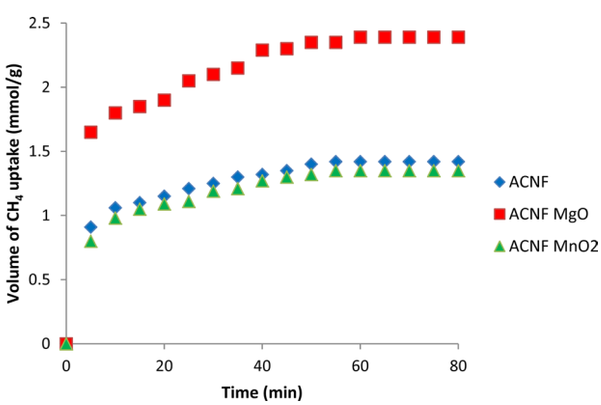

Fig. 7. Variation of the CH_4 uptake to reach equilibrium versus time on activated carbon nanofibers (ACNFs) with different types of metal oxides at 3.5 bar.

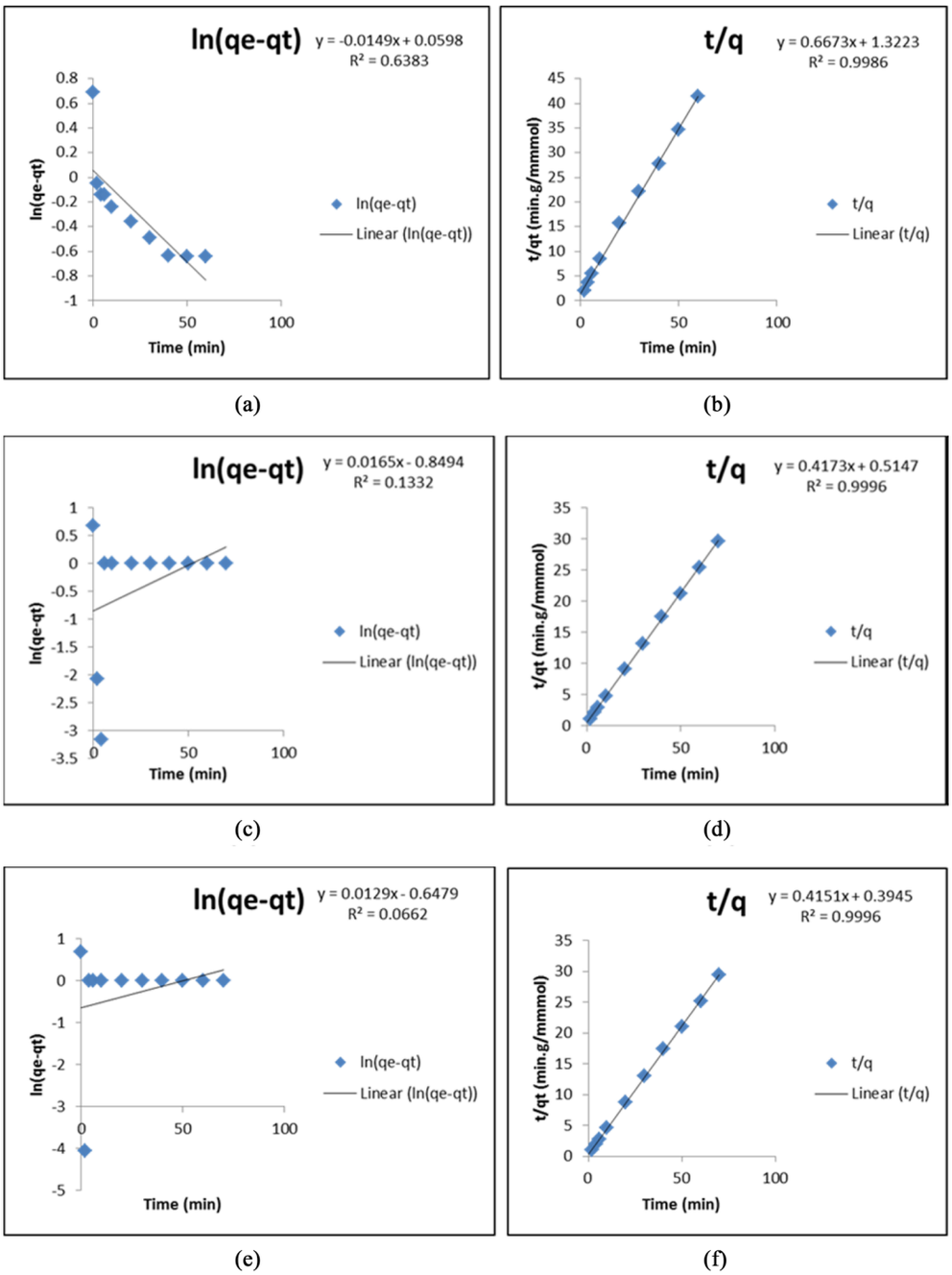

Fig. 8. Kinetics adsorption studies for the different types of ACNFs-based adsorbents. (a) Pseudo-first and (b) pseudo-second order of the pristine ACNFs; (c) pseudo-first and (d) pseudo-second order of the ACNF/MgO; and (e) pseudo-first and (f) pseudo-second order of the ACNF/MnO_2.

3.6. Kinetic studies of the ACNFs

The pseudo-first order and pseudo-second order for the CH_4 adsorption on the porous structure ACNFs were analyzed and plotted in Fig. 8 while the kinetic parameters are tabulated in Table 3. As shown in the table, the pseudo-second order had a greater coefficient correlation (R^2) in all the samples compared to the pseudo-first order kinetic model. It can be seen that R^2 of the pseudo-second order for the pristine ACNFs, ACNF/MgO, and ACNF/MnO_2 is 0.9986, 0.9996, and 0.9996, respectively, and they yield very good straight lines compared to the plot of the pseudo-first order. Additionally, the applicability of this model is strongly influenced by the ranges of time within the experimental data are monitored.

From this finding, it can be said that all the experimental data for CH_4 adsorption for the selected ACNFs are best fitted with

Table 3. The kinetics parameters of the pseudo-first order and pseudo-second order model for the pristine ACNFs, ACNF/MgO, and ACNF/MnO_2 at an initial pressure of 3.5 bar

Sample	Pseudo-first order		Pseudo-second order		
	k_1	R^2	k_2	q_e	R^2
ACNF	–0.0149	0.6383	1.4986	1.45	0.9986
ACNF/MgO	–0.0165	0.1332	2.3964	2.39	0.9996
ACNF/MnO_2	–0.0129	0.0662	2.4096	2.35	0.9996

ACNF, activated carbon nanofiber.

the pseudo-second order model, and these linear plots indicate the sorption kinetics of CH_4 on the mesoporous and microporous ACNFs. This model was determined as physical adsorption due to the formation of multilayers of CH_4 molecules on the ACNFs surface which starts as a monolayer adsorption and then turns into a multilayer form until the pores are fully occupied with CH_4 molecules. Moreover, this finding also corresponds to the adsorption kinetics of a CH_4 study conducted by Luo et al. [25] because they also found that porous carbon- based adsorbents obeyed the pseudo-second order kinetic model.

4. Conclusions

It is worth mentioning that ACNFs with different types of metal oxides in the PAN-based NFs can be successfully produced by electrospinning, followed by suitable activation conditions. In our experiment, ACNF/MgO had the highest surface area of up to 1893 $m^2 g^{-1}$ compared with the pristine and MnO_2-modified ACNFs. These results are supported by the fact that the incorporation of metal oxides in ACNFs exacerbate the pyrolysis process due to the catalytic effects of the metal oxides themselves. As the above characteristics are a concern, the magnesium oxide (MgO) nanoparticles had smaller particle sizes, which showed superiority over the pure ACNFs and ACNF/MnO_2. In other words, the addition of MgO into the precursor produced modified ACNFs with a higher SSA, which led to a higher catalytic activity. This finding highlights the potential of PAN-based ACNFs/MgO as a precursor for the preparation of the sustainable porous carbon for gas storage applications.

Conflict of Interest

No potential conflict of interest relevant to this article was reported.

Acknowledgements

The authors would like to acknowledge the financial support from the Ministry of Education Malaysia and Universiti Teknologi Malaysia under GUP grant (Q.J130000.2546.12H54 and Q.J130000.2546.16H29), Higher Institution Centre of Excellence (HiCOE) grant (R.J090301.7846.4J180) and Fundamental Research Grant Scheme (R.J130000.7846.4F929). The authors would also like to acknowledge the technical and management support from Research Management Centre (RMC), Universiti Teknologi Malaysia.

References

[1] Yusof N, Ismail AF. Post spinning and pyrolysis processes of polyacrylonitrile (PAN)-based carbon fiber and activated carbon fiber: a review. J Anal Appl Pyrolysis, **93**, 1 (2012). https://doi.org/10.1016/j.jaap.2011.10.001.

[2] Rios RB, Bastos-Neto M, Amora MR Jr, Torres AEB, Azevedo DCS, Cavalcante CL Jr. Experimental analysis of the efficiency on charge/discharge cycles in natural gas storage by adsorption. Fuel, **90**, 113 (2011). https://doi.org/10.1016/j.fuel.2010.07.039.

[3] Im JS, Park SJ, Kim TJ, Kim YH, Lee YS. The study of controlling pore size on electrospun carbon nanofibers for hydrogen adsorption. J Colloid Interface Sci, **318**, 42 (2008). https://doi.org/10.1016/j.jcis.2007.10.024.

[4] Yeoh WM, Lee KY, Chai SP, Lee KT, Mohamed AR. Effective synthesis of carbon nanotubes via catalytic decomposition of methane: Influence of calcination temperature on metal–support interaction of Co–Mo/MgO catalyst. J Phys Chem Solids, **74**, 1553 (2013). https://doi.org/10.1016/j.jpcs.2013.05.023.

[5] Alhasan S, Carriveau R, Ting DSK. A review of adsorbed natural gas storage technologies. Int J Environ Stud, **73**, 343 (2016). https://doi.org/10.1080/00207233.2016.1165476.

[6] Lee HM, Kang HR, An KH, Kim HG, Kim BJ. Comparative studies of porous carbon nanofibers by various activation methods. Carbon Lett, **14**, 180 (2013). https://doi.org/10.5714/CL.2013.14.3.180.

[7] Ucar N, Cavdar Z, Karatepe N, Altay P, Kizildag N. SO_2 adsorption capability of activated carbon nanofibers produced by different activation process parameters. J Text Apparel, **26**, 407 (2016).

[8] Othman FEC, Yusof N, Raffi AA, Hasbullah H, Aziz F, Salleh WNW, Ismail AF. Preparation and characterization of different loading of zinc oxide on activated carbon nanofibers. Malay J Anal Sci, **21**, 365 (2017).

[9] Yusof N, Rana D, Ismail AF, Matsuura T. Microstructure of polyacrylonitrile-based activated carbon fibers prepared from solvent-free coagulation process. J Appl Res Technol, **14**, 54 (2016). https://doi.org/10.1016/j.jart.2016.02.001.

[10] Ji L, Zhang X. Ultrafine polyacrylonitrile/silica composite fibers via electrospinning. Mater Lett, **62**, 2161 (2008). https://doi.org/10.1016/j.matlet.2007.11.051.

[11] Gliścińska E, Babeł K. Preparation of activated carbon fibres from electrospun polyacrylonitrile fibre mat and characterisation of their

chemical and structural properties. Fibres Text East Eur, **99**, 42 (2013).

[12] Huang ZM, Zhang YZ, Kotaki M, Ramakrishna S. A review on polymer nanofibers by electrospinning and their applications in nanocomposites. Compos Sci Technol, **63**, 2223 (2003). https://doi.org/10.1016/S0266-3538(03)00178-7.

[13] Sedghi A, Farsani RE, Shokuhfar A. The effect of commercial polyacrylonitrile fibers characterizations on the produced carbon fibers properties. J Mater Process Technol, **198**, 60 (2008). https://doi.org/10.1016/j.jmatprotec.2007.06.052.

[14] Hidayu AR, Mohamad NF, Matali MS, Sharifah ASAK. Characterization of activated carbon prepared from oil palm empty fruit bunch using BET and FT-IR techniques. Proceedia Eng, **68**, 379 (2013). https://doi.org/10.1016/j.proeng.2013.12.195.

[15] Nasri NS, Hamza UD, Ismail SN, Ahmed MM, Mohsin R. Assessment of porous carbons derived from sustainable palm solid waste for carbon dioxide capture. J Cleaner Prod, **71**, 148 (2014). https://doi.org/10.1016/j.jclepro.2013.11.053.

[16] Khalil KA, Sherif EM, Nabawy AM, Abdo HS, Marzouk WW, and Alharbi HF. Titanium carbide nanofibers-reinforced aluminum compacts, a new strategy to enhance mechanical properties. Materials, **9**, 399 (2016). https://doi.org/10.3390/ma9050399.

[17] Zheng JF, He A, Li J, Xu J, Han CC. Studies on the controlled morphology and wettability of polystyrene surfaces by electrospinning or electrospraying. Polymer, **47**, 7095 (2006). https://doi.org/10.1016/j.polymer.2006.08.019.

[18] Dadvar S, Tavanai H, Morshed M. Effect of embedding MgO and Al_2O_3 nanoparticles in the precursor on the pore characteristics of PAN based activated carbon nanofibers. J Anal Appl Pyrolysis, **98**, 98 (2012). https://doi.org/10.1016/j.jaap.2012.08.001.

[19] Tavanai H, Jalili R, Morshed M. Effects of fiber diameter and CO_2 activation temperature on the pore characteristics of polyacrylonitrile based activated carbon nanofibers. Surf Interface Anal, **41**, 814 (2009). https://doi.org/10.1002/sia.3104.

[20] Kimura Y, Kurumada M, Tamura K, Koike C, Chihara H, Kaito C. Laboratory production of magnesium sulfide grains and their characteristic infrared spectra due to shape. Astron Astrophy, **442**, 507 (2005). https://doi.org/10.1051/0004-6361:20052757.

[21] Zhang P, Li X, Zhao Q, Liu S. Synthesis and optical property of one-dimensional spinel $ZnMn_2O_4$ nanorods. Nanoscale Res Lett, **6**, 323 (2011). https://doi.org/10.1186/1556-276X-6-323.

[22] Sun M, Lan B, Lin T, Cheng G, Ye F, Yu L, Cheng X, Zheng X. Controlled synthesis of nanostructured manganese oxide: crystalline evolution and catalytic activities. CrystEngComm, **15**, 7010 (2013).

[23] Thiagarajan S, Tsai TH, Chen SM. Electrochemical fabrication of nano manganese oxide modified electrode for the detection of H_2O_2. Int J Electrochem Sci, **6**, 2235 (2011).

[24] Wan Isahak WNR, Che Ramli ZA, Mohamed Hisham MW, Yarmo MA. Magnesium oxide nanoparticles on green activated carbon as efficient CO_2 adsorbent. AIP Conf Proc, **1571**, 882 (2014). https://doi.org/10.1063/1.4858766.

[25] Luo J, Liu Y, Jiang C, Chu W, Jie W, Xie H. Experimental and modeling study of methane adsorption on activated carbon derived from anthracite. J Chem Eng Data, **56**, 4919 (2011). https://doi.org/10.1021/je200834p.